

Effect of Basicity on the Hydrolysis of the Bi(III) Aqua Ion in Solution: an Ab Initio Molecular Dynamics Study

Regla Ayala,^{†,§} José Manuel Martínez,[‡] Rafael R. Pappalardo,[‡] Keith Refson,^{¶,||}
and Enrique Sánchez Marcos^{*,‡}

[†]*Universidad de Sevilla, CSIC, ICMSE*

[‡]*Universidad de Sevilla, Departamento Química Física, 41012 Seville, Spain*

[¶]*Royal Holloway University of London, Egham Hill, Egham, Surrey TW20 0EX, United
Kingdom.*

[§]*Departamento Química Inorgánica, 41012 Seville, Spain*

^{||}*ISIS Facility, Science and Technology Facility Council, Harwell Science Campus, Didcot,
OX11 0QX, UK*

E-mail: sanchez@us.es

Abstract

Hydrolysis of the Bi(III) aqua ion under a range of solution conditions has been studied by means of ab initio molecular dynamics simulations. While the Bi(III) aqua ion is stable in pure water, there is an increasing degree of hydrolysis with the number of hydroxide anions in the medium. This is accompanied by a monotonic decrease of the total coordination number to an asymptotic value of ~ 6 , reached under extreme basicity conditions. Comparison of the simulated Bi(III) hydrolyzed species with the experimental species distribution at different degrees of basicity suggests that at the PBE/DFT level of theory here employed, liquid water shows an overly acidic character. Predictions of theoretical EXAFS and XANES spectra were generated from the AIMD trajectories for different Bi hydrolyzed species, $[\text{Bi}(\text{HO})_m(\text{H}_2\text{O})_n]^{3-m+}$, $m=0-3$ and $n=7-2$. Comparison with available experimental spectra is presented. Spectral features joined to the degree of hydrolysis and hydration are analyzed.

Introduction.

Although ion hydration is a central topic of solution chemistry, the description of highly-charged ion-water interactions remains a challenge, particularly for some multivalent cations involved in a series of hydrolysis reactions and polynucleation processes.¹⁻⁶ This is the case of Bi(III) in water, which plays important roles in chemistry and medicine; for example as an antimicrobial and anticancer agent or in radio-therapy, to name just a few.^{2,3,5-18} The aqua ion, $[\text{Bi}(\text{H}_2\text{O})_n]^{3+}$, was characterized by Näslund et al.¹⁷ from acidic solutions of its triflate salt. These authors emphasized the importance of hydrolysis in its solution chemistry. The strong propensity of Bi(III) to suffer hydrolysis in aqueous solution derives from its rather complex chemistry in water. Hydrolyzed species occur in both monomeric, $[\text{Bi}(\text{OH})_m(\text{H}_2\text{O})_n]^{3-m}$, and polymeric, $[\text{Bi}_p(\text{OH})_m(\text{H}_2\text{O})_n]^{3p-m}$ species.¹ Hydrolysis, polymerization and anion complexation are all involved as a function of the concentration, degree of acidity, counterions and supporting electrolytes. Tooth et al.¹⁹ carried out a study on the nature and stability of Bi(III) aqueous complexes under natural hydrothermal conditions, characterizing monomeric species bearing up to four OH^- groups.

Figure 1 shows the species distribution diagram of the aqueous Bi(III) ion as a function of pH.²⁰ Monomeric species appear only at low Bi(III) concentrations and no evidence of polynuclear species formation in highly dilute solution ($\sim 10^{-5}$ M) has been found.^{5,6,19,20} Therefore, the Bi(III) concentration determines which are the main species present: polynuclear species at high or moderate Bi(III) concentrations and mononuclear species at low concentrations. The aqueous oxo species (BiO^+) is not usually included in distribution species diagrams, due in part to the difficulty of discriminating between O^{2-} and OH^- ligands.¹ The BiOX species in water can be also formulated as $\text{Bi}(\text{OH})_2\text{X}$,¹⁰ X^- being the salt counterion (which is chosen to be non-complexing, or at least very weakly complexing). Nonetheless, the presence of BiOX species can not be disregarded. The formation of BiOCl ,¹¹ BiOClO_4 ^{9,13,17} and BiONO_3 ,^{11,12} species, have all been reported, the last two being very insoluble.¹¹ Therefore, the degree of hydrolysis is lower due to the nitrate or chloride

complexing ability with Bi(III) as mononuclear species.^{12–16}

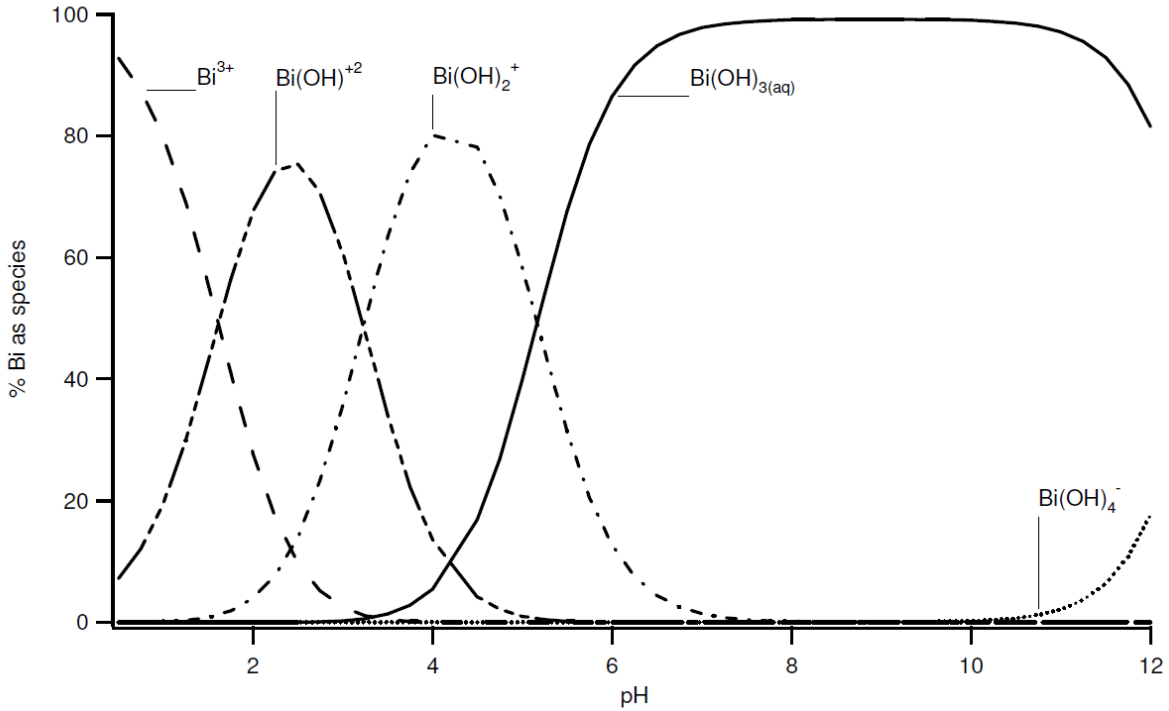
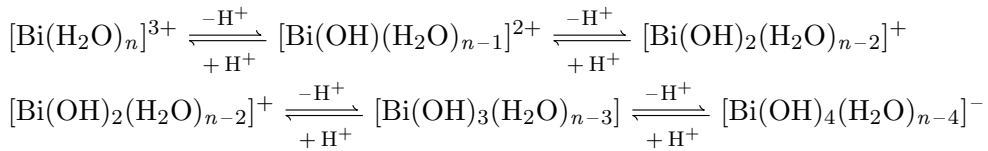


Figure 1: Experimental species distribution diagram of Bi(III) aqueous solutions at room temperature taken from Ref.[20].

The species distribution is governed by the equilibrium constants associated with the hydrolysis processes⁹ which allow the formulation of the complex equilibria



involving monomeric species under particular pH conditions, as detailed in Figure 1.^{1,20}

The theoretical study of hydrolysis processes and determination of the dominant species as a function of the pH medium is not easy. In a previous quantum mechanical (QM) study²¹ on Bi(III) aqueous solutions using a semi-continuum solvent model, the analysis of the equilibria and the different structures involved showed a decrease in the coordination number as hydrolysis processes proceed. Starting from the octa-hydrate, $[\text{Bi}(\text{H}_2\text{O})_8]^{3+}$, a threefold coordination was observed when a degree of hydrolysis of 3 (understood as the number of hydroxyl ligands in the first solvation shell) was reached, $[\text{Bi}(\text{OH})_3]$. However,

the analysis of these equilibrium structures could only be interpreted assuming that solvent effects were provided by a continuum dielectric without accounting for a particular acid or basic medium. Thus, the differences arose only from the number of water molecules in the cluster without any formal change in the chemical nature of the bulk solvent. QM methodology based on the Self Consistent Reaction Field²² does not allow us to connect the number of OH⁻ ligands in [Bi((OH)_m(H₂O)_n]^{3-m} clusters with the medium conditions. That is, the OH-ligand number was imposed and the evaluation of the optimum number of water molecules in the [Bi(OH)_m(H₂O)_n]^{(3-m)+} ion was subsequently obtained by changing (*n*). In other words, once the degree of hydrolysis (*m*) was fixed, the total coordination number (*n* + *m*) was determined. The present work expands on the previous static QM view by modeling the solvent at the molecular level, by considering now the evolution of the Bi(III) species as a function of medium conditions. To this aim ab initio molecular dynamics (AIMD) simulations become an appropriate tool. In a previous work²³ on the Po(IV) hydration, medium conditions were modeled by specifying the initial configuration, that is, starting from partially or fully hydrolyzed aqua ion species, but retaining the same number of atoms in the simulation box. Every hydroxyl group in the initial Po(IV) coordination sphere was compensated by an extra proton in the bulk ([Po(OH)_m(H₂O)_n]^{(4-m)+} + *m* H⁺). The starting clusters considered (*m*=0, 2 and 3) converged to a similar equilibrated species distribution.²³

In the present case, we undertake the analysis of the evolution of Bi(H₂O)_n³⁺ aquaion and some of its hydrolyzed forms as a function of the number of hydroxide anions present in bulk water. The AIMD simulations allow us to follow the chemical evolution of the Bi(III) species and its bulk environment. The goal of determining the changes induced in the dominant species in solution on the addition and removal of proton species in the medium is within current capabilities. The structural analysis of AIMD trajectories provides valuable information on the connection between the degree of basicity of the medium and the number of OH⁻ ligands in the close environment of the Bi(III) ion. This work is therefore a first step in the use of AIMD simulations to evaluate how solvent conditions alter the population of

hydrolyzed species of monomeric Bi(III) aquaion in aqueous solutions. It must be pointed out that this theoretical study can be carried out at a qualitative level given that the pH values, as experimentally given in Figure 1, can not be obtained in our case with the methodology employed. Therefore, the speciation distribution diagram of the different Bi(III) monomeric species is only a qualitative guide of species detected under different media, an index of their appearance sequence when the basicity conditions are changed in the medium.

Although DFT description of liquid water is not fully satisfactory because there is no functional that can simultaneously describe its structure, dynamics and thermodynamics,²⁴⁻³⁰ among GGA functionals, PBE is capable of predicting the energetics of water clusters reasonably well.^{24,29} It is worth noting that in this study we are dealing with highly-charged hydrated ion solutions where the ion-water interactions are significantly larger than the energies associated to the water-water interactions. This fact gives us more confidence in the description of the closest Bi(III) environment using PBE. Even more, an important point for the proper description of hydrolysis processes is the average number of hydrogen bonds. For PBE water, the value is 3.7,³⁰ which is quite close to the experimental estimation (3.5) at ambient conditions.³¹

The behavior of OH^- in water has been the central subject of many theoretical studies and we refer to recent reviews on this topic³²⁻³⁴ which reveal that the DFT level of theory is inadequate for an accurate description of the aqueous hydrolysis structure and thermodynamics of hydroxide anions. In the present study we focus our attention on the Bi(III) aquaion and its hydrolyzed forms which are mediated by hydroxyl ligands, rather than by the hydroxide anions. The relative errors of the DFT energetics will be smaller in the highly polarized ligand environment than in bulk aqueous solution, so it is reasonable to suppose that the effect will be less severe.

From an experimental side, X-ray absorption spectroscopies (EXAFS and XANES) are appropriate techniques to help in the structural elucidation of the species in solution.³⁵ However, this complex behavior makes difficult the collection of XAS spectra of the $[\text{Bi}(\text{H}_2\text{O})_m]^{3+}$

aqua ion, an important reference for the follow up of the chemical changes induced by the medium. Näslund et al.¹⁷ carried out a systematic EXAFS study on Bi(III) solvation in several solvents, including water, and their related solvated crystal. The difficult issue is to discriminate the presence of one or several Bi(III) species in solution contributing to the global EXAFS signal. Tooth et al.¹⁹ carried out a systematic XAS study on monomeric $[\text{Bi}(\text{H}_2\text{O})_n(\text{OH})_m]^{3-m}$ in water under hydrothermal conditions which can also be taken as a valuable experimental reference. In this sense, it would be of general interest to simulate XAS spectra from the structural information provided by our MD simulations. Because the chemical species involved are well characterized, the XAS spectrum and the solution structure can be easily correlated, and contributions to the total signal identified.³⁶⁻⁴⁰



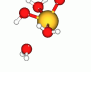
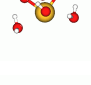

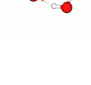
Methodology.

Simulation Protocols.

Plane-wave AIMD simulations were performed using the Car-Parrinello scheme⁴¹ as implemented in the CPMD code⁴² The NVT ensemble at a temperature of 350 K using a Nosé-Hoover chain of thermostats on the ionic degrees of freedom was employed.⁴³⁻⁴⁵ For an initial period of 0.6 ps the timestep was set at 0.060 fs while the electronic system relaxed towards the ground state, switching to 0.097 fs thereafter. The fictitious mass of the additional electronic degrees of freedom was 400 a.u. Periodic boundary conditions were applied to a cubic simulation box of side 13.136 Å. Vanderbilt ultrasoft pseudopotentials⁴⁶ (USP) were used to describe the interactions between the ionic cores and the valence electrons. A plane wave cutoff of 30 Ry was used. The electronic wavefunction was solved using DFT with the PBE exchange-correlation functional.⁴⁷ Oxygen and hydrogen pseudopotentials were taken from standard libraries, but for Bi we generated a new pseudopotential using a $6s^26p^2$ reference configuration and $r_c = 2.0a_0$. The use of two projectors per angular momentum channel and the direct generation of fully-local projectors have proven the good

behavior of this set of pseudopotentials.⁴⁸ This was tested against an accurate reference USP by computing forces for a single hydrated Bi(III) in crystalline Bi₂O₃ yielding a standard deviation of 0.016 eV/Å. To check the coupling of this new pseudopotential with the rest of QM elements employed in the Bi(III) clusters, we have optimized a set of hydrolyzed species, [Bi(OH)_m(H₂O)_n]^{(3-m)+}, and compared with the optimized structures obtained for the same species in our previous DFT(MPW1PW91) study using Gaussian basis sets.²¹ Table 1 gives the Bi–O(OH) and Bi–O(H₂O) distances and the optimized geometries for clusters having up to four OH groups. It is shown a satisfactory agreement that supports the good performance of the Bi pseudopotential proposed.

Table 1: Average Bi-O(OH) and Bi-O(H₂O) distances taken from Ref. 21 for quantum mechanical optimizations (MPW1PW91/Gaus.) and from PBE and Plane-wave using the ultrasoft pseudopotential developed in this study.

Structure	Method	d(BiO _{H₂O})/Å	d(BiO _{H₂O})/Å
 7+0	MPW1PW91/Gaus.	3×2.43, 2×2.47, 2×2.49	—
	PBE/PW	2×2.41, 2.42, 2.44, 2.46, 2.47, 2.48	—
 5+1	MPW1PW91/Gaus.	2×2.46, 2.47, 2.52, 2.54	2.03
	PBE/PW	3×2.45, 2.51, 2.53	2.04
 3+2	MPW1PW91/Gaus.	2.48, 2.49, 2.91	2.05, 2.06
	PBE/PW	2.47, 2.48, 2.82	2.06, 2.07
 3+3	MPW1PW91/Gaus.	2.66, 2.68, 2.74	2.11, 2.14, 2.18
	PBE/PW	2.64, 2.65, 2.69	2.12, 2.15, 2.19
 2+3	MPW1PW91/Gaus.	2.64, 2.69	2.10, 2.13, 2.15
	PBE/PW	2.63, 2.65	2.11, 2.14, 2.16
 1+4	MPW1PW91/Gaus.	3.52	2.14, 2.15, 2.22, 2.28
	PBE/PW	3.53	2.14, 2.15, 2.21, 2.26

The thermalization and production periods were 8.6 and 40 ps long, respectively.

Hydrolysis events were identified using the following criteria:⁴⁹ i)for each O atom, the H atoms being at 1.2 Å or closer are assigned to that oxygen atom; ii)each H atom that

lengthens the O-H distance by more than 1.2 Å is considered as temporary hydrolyzed and, therefore has undergone a hydrolysis event. The number of ligands in the first solvation shell were obtained as follows: all the O atoms at a Bi-O distance shorter than the minimum in the depletion range (2.75-3.4 Å) of the Bi-O radial distribution function (RDF) were considered to belong to the first solvation shell. The H atoms bonded to these O atoms were found and assigned as previously explained. The analysis was done over all the production periods.

AIMD simulations

The first set of AIMD simulations consists of an octahydrate $[\text{Bi}(\text{H}_2\text{O})_8]^{3+}$ surrounded by 56 water molecules (simulation 1, see Table 2). The initial configuration was obtained as follows: First of all, a classical MD simulation of the system in which the octahydrate was treated as a rigid unit was run using the geometry of the octahydrate taken from previous quantum mechanical calculations.²¹ Water molecules were described by the SPC/E force field.⁵⁰ A classical MD trajectory of 200 ps was produced and the final configuration used as an input for the subsequent AIMD thermalization. To avoid any hydrolysis event related to an out-of-equilibrium initial configuration, the octahydrate geometry was constrained during the first 6000 steps of the AIMD simulation.

To explore the consequences of an increase in basicity, a second set of simulations was performed starting from the final configuration of the previous one but with one, two and three protons removed from the simulation box (simulations 2A, 2B and 2C, respectively, see Table 2). These protons were chosen to be as far as possible from the Bi(III) ion.

The third set of simulations started from the final configuration of simulation 2C, corresponding to a $[\text{Bi}(\text{OH})_3(\text{H}_2\text{O})_3]$ hydrolyzed species, with a further one, two and three protons removed from the simulation box (simulations 3A, 3B and 3C, respectively, see Table 2) in order to determine the largest degree of hydrolysis that can be reached under extreme basicity.

Finally, the fourth set of simulations started from the $[\text{BiO}]^+$ species. A double depro-

tonation on the same O atom of a water molecule was forced. The initial configuration was obtained from a classical MD where the $[\text{BiO}]^+$ species was treated as a rigid unit. The AIMD simulation started considering the $[\text{BiO}]^+$ cluster as a rigid unit.

The addition of protons to the medium was not considered because hydrolysis events were not observed in simulation 1.

Simulated EXAFS and XANES spectra

From the MD trajectory, a set of 400 snapshots are evenly taken for simulating the EXAFS and XANES spectra, as in previous studies of metal ions in solution.^{37–40,51,52} The Bi L_3 -edge EXAFS spectrum was computed by averaging the individual $\chi_s(k)$ calculated for each snapshot. Then, disorder arises from the instantaneous non-symmetric arrangement of each structure and from summing over a statistically significant number of snapshots.

$$\chi(k) = \frac{1}{N_s} \sum_s^{N_s} \chi_s(k) = \frac{1}{N_s} \sum_s^{N_s} \sum_j^{paths} \frac{N_j S_0^2}{k R_j^2} |f_j^{eff}(k, R_j)| \sin(2kR_j + \varphi_j(k)) \times e^{-2R_j/\lambda(k)}$$

where the summation goes over all paths j . In this equation N_j is the coordination number, S_0^2 the amplitude reduction factor, R_j the path length, f_j^{eff} the curved-wave backscattering amplitude, φ_j the phase-shift, λ the mean free path.⁵³

This procedure differs from the original EXAFS equation in the fact that the Debye-Waller factors are replaced by a sum over N_s structures (snapshots): where s goes over the structures obtained from the sampling, and j goes over all the paths generated from each structure, restricted to a maximum path-length of 6 Å and 4-legs. Regarding the sphere radius (R_{cut}) needed to account all significant backscattering contributions to the EXAFS signal, it was tested that the consideration of one coordination shell around the Bi(III) is enough. Similar simulated spectrum is obtained if R_{cut} is increased to account for two coordination shells. The computation of the EXAFS and XANES spectra for a

given structure was carried out by means of the FEFF code (version 9.6) developed by Rehr’s group.⁵³ This program calculates both XAS spectra using ab initio self-consistent real space multiple scattering. The Hedin-Lundqvist exchange-correlation potential was chosen to compute the electron density distribution within the self-consistent field approach. In the case of XANES computations, a full multiple scattering for a cluster centered on the Bi atom was used.

Sample input files employed to calculate the simulated spectra are given in the Supporting Information (SI).

The use of snapshots coming from AIMD trajectories implies that simulated spectra have an ab initio origin. This is to say, no experimental information has been used in the XAS spectra building. To double the relationship between an experimental EXAFS spectrum and structure one may build a set of intermolecular potentials which produces the same structural parameters than the fitted ones.⁵⁴ This is a good test on the influence of other structural and spectroscopical factors on the final signal. To carry out this test we need to develop a trajectory where the basic structural characteristics of the Bi(III) environment given by the experimental fitting are reproduced. Thus, a Bi-water intermolecular potential specifically fitted to reproduce the structural data reported by Näslund et al.¹⁷ has been built. This “ad hoc” Bi-water potential is based on a Morse potential developed to describe the metal cation-water interaction in such a way that gives the Naslund et al’s data, i.e. $R_{\text{Bi-O}}=2.408$ Å, coordination number 8, and a Debye-Waller (DW) factor for the Bi-O paths of 0.0132 Å².

$$U_{\text{Bi-O}}(r) = E_0[(1 - e^{-k(r-r_0)})^2 - 1] \tag{1}$$

where, $E_0=57.1$ kcal/mol, $r_0=2.834$ Å and $k=0.67518$ Å⁻¹. Water-water interactions were described by the SPC/E water model.

Results and Discussions.

Table 2 collects the summary of the AIMD simulations considered in this work and shows both the initial and final species distributions as a function of the medium. RDFs for each of the simulations are plotted in Fig. 2.

Table 2: Summary of the sets of simulations run in this study. The dominant species in the distribution are in bold.

Set of simulations	Initial configuration			Representative hydrated species ion + 1 st solvation shell
	ion + 1 st solvation shell	n° of bulk H ₂ O	n° of bulk OH ⁻	
1	[Bi(H ₂ O) ₈] ³⁺	56	0	[Bi(H ₂ O) ₇] ³⁺
2A	[Bi(H ₂ O) ₇] ³⁺	56	1	[Bi(OH)(H ₂ O) ₅] ²⁺
2B	[Bi(H ₂ O) ₇] ³⁺	55	2	[Bi(OH) ₂ (H ₂ O) ₄] ⁺
2C	[Bi(H ₂ O) ₇] ³⁺	54	3	[Bi(OH) ₃ (H ₂ O) ₃]
3A	[Bi(OH) ₃ (H ₂ O) ₃]	57	1	[Bi(OH) ₄ (H ₂ O)] ⁻ , [Bi(OH) ₄ (H ₂ O) ₂] ⁻
3B	[Bi(OH) ₃ (H ₂ O) ₃]	56	2	[Bi(OH) ₄ (H ₂ O)] ⁻ , [Bi(OH) ₅] ²⁻
3C	[Bi(OH) ₃ (H ₂ O) ₃]	55	3	[Bi(OH) ₅ (H ₂ O)] ²⁻ , [Bi(OH) ₆] ³⁻
4	[BiO] ⁺	63	0	[Bi(OH) ₂ (H ₂ O) ₃] ⁺ , [Bi(OH) ₂ (H ₂ O) ₄] ⁺

Radial Distribution functions (RDFs).

Simulation 1 shows a well defined peak centered at ~ 2.5 Å which corresponds to the Bi-O_{H₂O} contributions. In going from that simulation to simulation 2C the main change is the appearance of the Bi-O_{OH} contributions. The Bi-O_{OH} interaction is stronger than the Bi-O_{H₂O} one making the BiO_{OH} distances shorter than those of Bi-O_{H₂O}. The intensities of these two peaks change from simulations 2A to 2C due to the increase in the number of hydroxyl ligands and the simultaneous decrease in the number of H₂O molecules around the Bi(III) ion. The total coordination number also decreases when going from simulation 1 (7) to simulation 2B, but it does not change in simulations 2B and 2C (5.5-6). As previously found, the hydrolysis processes are associated with dehydration events.^{21,23,55-57} Starting from the Bi(III) aqua ion, the increase in the basicity leads to an increase in the degree of hydrolysis of the Bi(III) aqua ion complexes, as well as to a decrease in its global coordination number.

In the case of simulations 3A-3C, which start from the hydrolyzed species [Bi(OH)₃(H₂O)₃], there is a first Bi-O peak associated to the Bi-O_{OH} interaction. A small hump at around 2.8 Å can be identified for simulation 3A which corresponds to Bi-O_{H₂O} interaction. A shift of the first peak towards longer distances is observed as the removal of the protons proceeds (from simulation 3A to 3C). This elongation is due to the relative position of the hydroxyl ligands and will be explained in detail in Section 3.2. The Bi-O coordination number is around 5-6, whereas in simulations 2 it is closer to 6.

Finally the Bi-O RDF of simulation 4 is similar to that of simulation 2B. This might be surprising considering that simulation 4 starts from the BiO⁺ species. If the bismuthyl cation was stable, the usual character of a metal-oxo bond would result in a well defined peak in the Bi-O RDF at short Bi-O distance. But that is not the case, and the broadened peak shows instability of the Bi-oxo species in solution. Simulations 2B and 4 both consist of 1 Bi, 64 O and 126 H with a total charge of +1, but, structurally, started from completely different initial states. However both converge to very similar chemical composition characterized by

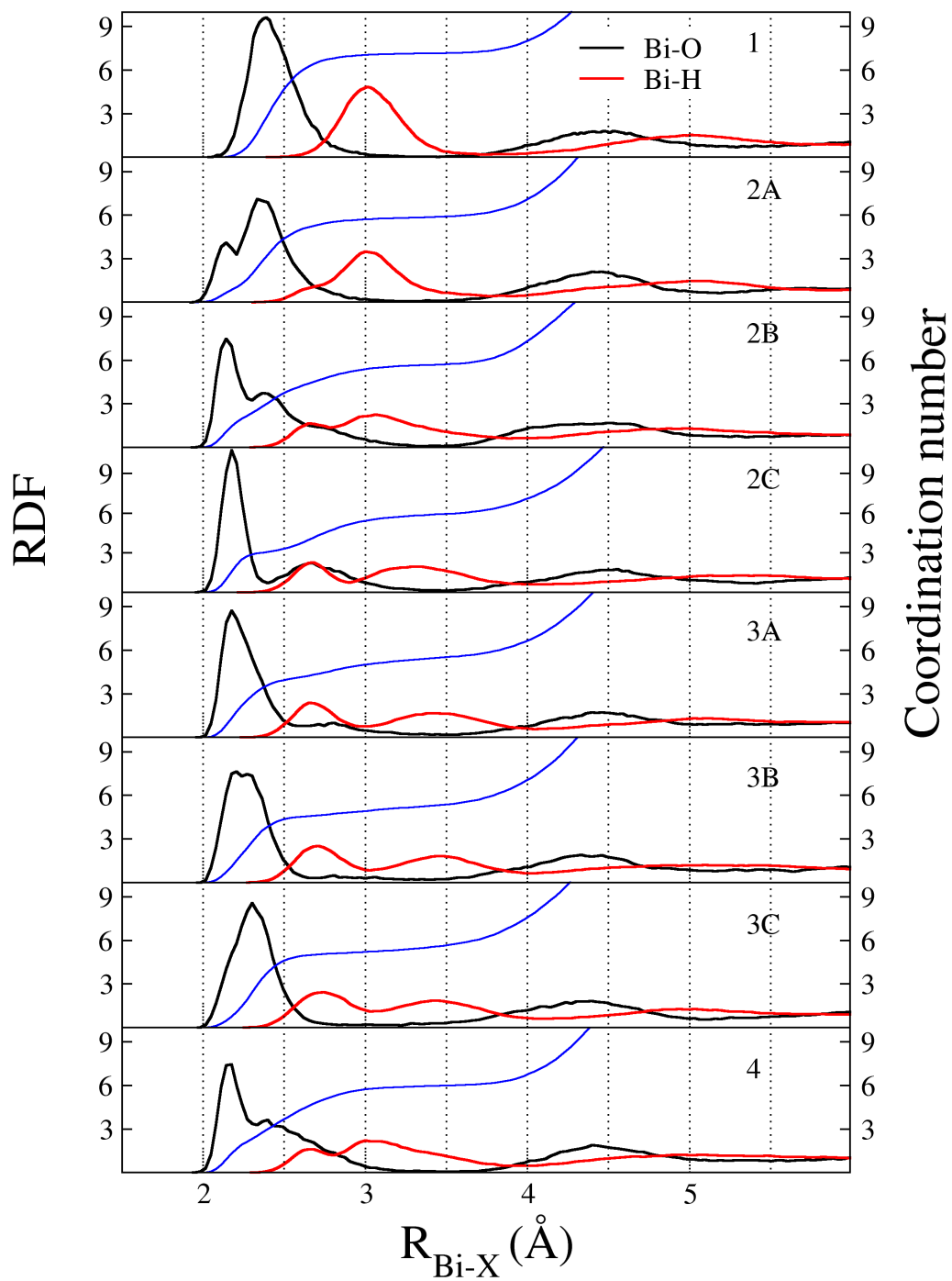


Figure 2: Bi-O RDFs (black) along with their running integration numbers (blue) and Bi-H RDFs (red) for simulations 1-4.

almost identical Bi-O RDFs. This demonstrates that our simulation times were sufficiently long to exceed the characteristic timescales of hydrolysis events and achieve configurational convergence.

The Bi-H RDFs support this analysis. For simplicity, running integration number curves for hydrogen are not included in Figure 2. The first peak is split into two by the hydrolysis events previously discussed when going from simulation 1 to 2C. The peak at shorter distances corresponds to the H_{OH} atoms whereas the second one is due to the H_{H_2O} atoms. Bi-H RDFs of simulations 3A-3C are similar, although a slight shift toward longer distances occurs with the removal of protons. As expected, Bi-H RDF of simulation 4 is alike to simulation 2B.

Due to the peculiar shape of RDF series, we have performed an RDF error analysis for the Bi-O pair in the cases of simulations 1 and 2A. For both pair distribution functions, Figure 1 of SI includes the estimation of the standard error of the mean (SEM) for each value of r , that is, in addition to $g(r)$ distribution, $g(r) \pm SEM(r)$ lines have been included as well. This is a measure of the dispersion of values around the mean $g(r)$ values. For computing of $SEM(r)$, the blocking method of Flyvberg and Petersen⁵⁸ has been employed. Results show the consistency of our trajectories.

Once the RDFs have been analyzed, we can supply a detailed picture of the set of species involved in solution under different degree of hydrolysis.

The evolution of hydroxide anion in our simulations leads to a quick transformation of these ions in hydroxyl ligands in the Bi(III) first coordination shell. We have included in SI (Figure 2) a comparison between $O_{OH}-O_{H_2O}$ RDF of aqueous solutions containing OH^- ³² and the RDF of the same pair of the $[Bi(OH)(H_2O)_5]^{2+}$ solution. In this case the hydroxyl ligand is immersed in a metal complex which certainly induces a strong asymmetry in the water distribution. For this reason, apart from the total RDF, we have plotted an RDF where oxygen atoms belonging to the first-shell water molecules have been excluded. Likewise, for completeness reason the $O_{OH}-O_{H_2O}(1st.shell)$ RDF is also included in Figure 2 of SI. This

total RDF is only partially similar to the RDFs of OH^- in water.³²⁻³⁴ The peaks are shifted to longer R because the hydrogen bonds formed by the hydroxyl ligand are weaker than those of the OH^- . Contrarily, the Bi(III)-monohydrolyzed RDF is more similar to the structure of the OH^- surface water clusters obtained by Crespo et al.⁵⁹ This is due to the fact that one half of the sphere centered in the hydroxyl oxygen atom is controlled by the Bi(III) and not by the OH^- anion by itself.

First coordination shell analysis.

Simulation 1 starts with the aqua ion $[\text{Bi}(\text{H}_2\text{O})_8]^{3+} + 56 \text{H}_2\text{O}$ and ends at the $[\text{Bi}(\text{H}_2\text{O})_7]^{3+} + 57 \text{H}_2\text{O}$. No hydrolysis events were observed during the 40 ps simulation, just the loss of one water molecule from the first hydration shell at the fifth picosecond. Since that event, the heptahydrate is the representative species along the simulation, suffering short transient events involving first shell water exchanges. Analysis of EXAFS spectra of Näslund et al.¹⁷ uses a fix coordination number of 8 in an aqueous solution highly concentrated in perchloric acid to prevent aqua ion hydrolysis and polymerization phenomena.¹ To obtain a good fitting, their structural model included the presence of perchlorate anions in the first coordination shell and contributions of second-shell water molecules. Our simulation conditions correspond formally to about a 1 M Bi(III) aqueous solution without counterions which could be responsible in part of the disagreement in the coordination number of the aqua ion. Rode and coworkers⁶⁰ using an ab initio quantum mechanical charge field molecular dynamics (QMCF-MD) approach propose a 9-fold coordination with a maximum probability of the Bi-O distance at 2.51 Å. We will reexamine this point in the discussion of the EXAFS results.

When one proton was removed from the simulation box (simulation 2A), the system evolved as expected from our previous QM calculations,²¹ that is, one hydrolysis event is observed together with the loss of one water molecule, yielding the $[\text{Bi}(\text{OH})(\text{H}_2\text{O})_5]^{2+}$ aggregate at the thermalized situation. Subsequent hydrolysis processes were favored when

two protons were removed (simulation 2B). Starting from the aqua ion, a degree of hydrolysis of 2 was reached involving mainly two species with different number of water molecules: $[\text{Bi}(\text{OH})_2(\text{H}_2\text{O})_3]^+$ and $[\text{Bi}(\text{OH})_2(\text{H}_2\text{O})_4]^+$, the average coordination number for this system becoming 5.6.

Although a mechanistic study of the OH^- diffusion in these solutions is not the central objective of this work, we have qualitatively examined how evolves the initial OH^- anions placed on the box boundary in the set of simulations B. Grotthuss diffusion^{33,34} easily favored the system reorganization and equilibration during the first picoseconds of simulations. Figure 3 displays time evolution of the representative aggregates found in simulations 2C, 3A and 3C during the simulation.

The removal of a third proton (simulation 2C, see top of Figure 3) leads to more hydrolyzed clusters, $[\text{Bi}(\text{OH})_3(\text{H}_2\text{O})_n]$, being the hydration degree between 2 and 4, and the mean coordination number 6. Although hydrolysis and dehydration are coupled, when passing from simulation 2B to 2C a higher degree of hydrolysis does not imply the loss of more water molecules. This suggests an asymptotic limit for the coordination number of Bi(III) ion in aqueous solutions around 6.

In our previous quantum mechanical study,²¹ we found that when two or three OH^- groups become part of the first solvation shell of the Bi(III) they avoid a *trans* arrangement among them. The water molecules in a *trans* position to the hydroxyl ligands lengthen their Bi-O distances with respect to the remaining water molecules in the cluster. This behaviour is also found in simulations 2B and 2C and illustrated in Table 1.

To remove a fourth proton, the final configuration of simulation 2C was chosen as starting point. Its removal in simulation 3A leads to the evolution shown in the middle of Figure 3, where the main representative species are $[\text{Bi}(\text{OH})_4(\text{H}_2\text{O})]^-$ and $[\text{Bi}(\text{OH})_4(\text{H}_2\text{O})_2]^-$. These species were not considered in our previous study because we evaluated up to a maximum degree of hydrolysis of 3. However, they appear in the experimental species distribution diagram of Figure 1 at extreme alkaline conditions.¹⁹ When two and three protons (sim-

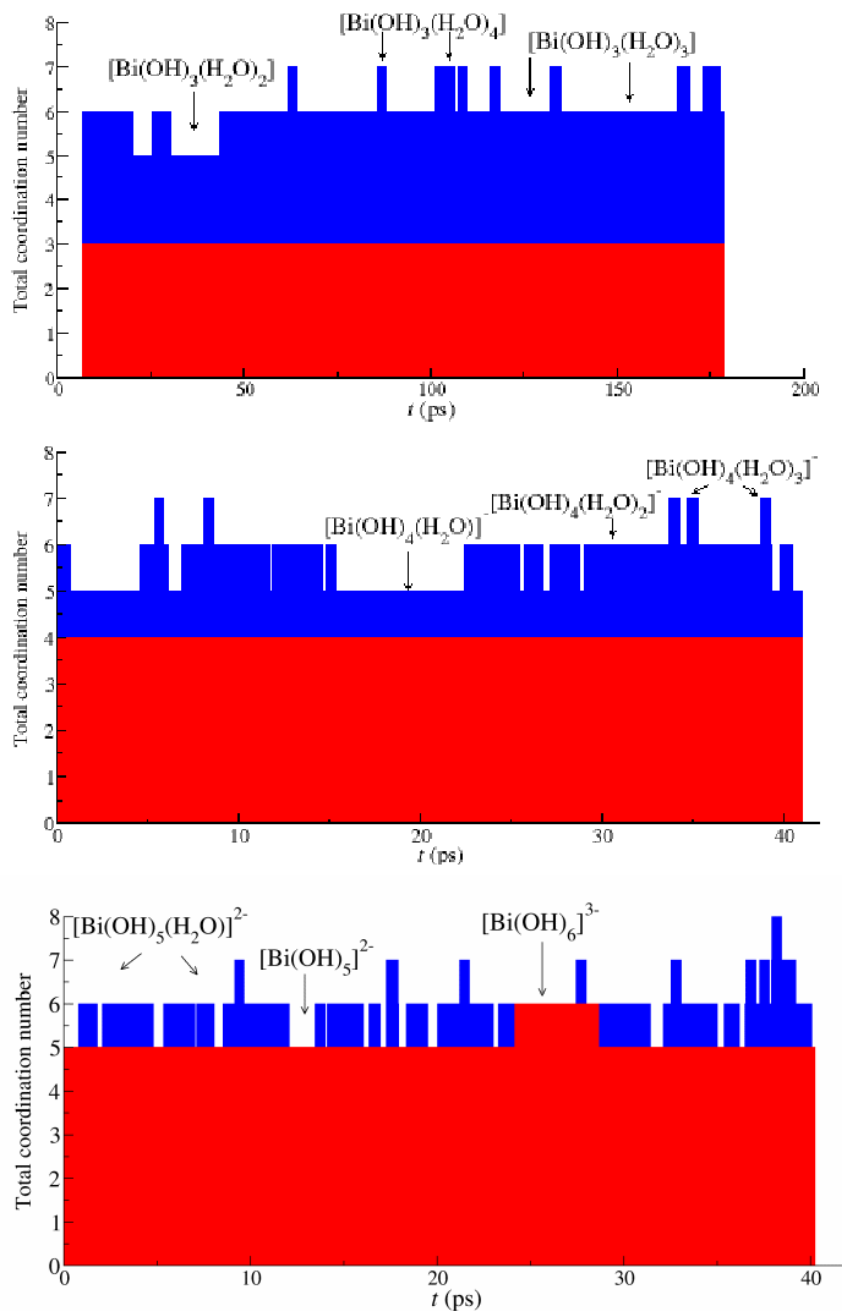


Figure 3: Time evolution (bar charts) of the Bi(III) environment in terms of number of water (blue bars) and hydroxyl ligands (red bars) along simulations 2C(top), 3A(middle) and 3C(bottom). Total bar height gives the total coordination number, partial coordination number for OH^- and H_2O are represented by the respective heights of blue and red bars.

ulations 3B and 3C, respectively) were removed from the final configuration of simulation 2C, both situations lead to highly hydrolyzed species, $[\text{Bi}(\text{OH})_5]^{2-}$, $[\text{Bi}(\text{OH})_6]^{-3}$ and some hydrated forms of them. Bottom of Figure 3 shows the evolution of simulation 3C where $[\text{Bi}(\text{OH})_5(\text{H}_2\text{O})]^{2-}$ is dominant although $[\text{Bi}(\text{OH})_5]^{2-}$ and $[\text{Bi}(\text{OH})_6]^{3-}$ are present along the simulation.

Although our results show the correct trend, there is an overestimate of the degree of hydrolysis, likely due to an incorrect balance between H bonding and water coordination that gives rise to a too acidic water model. The absence of counterions may also influence the observed behavior.¹²⁻¹⁶ The removal of 6 protons from simulation 1 to simulation 3C can be regarded as an extreme scenario of alkaline conditions collected in Fig. 3 (bottom).

In our previous work²¹ the possibility of four or more OH^- ligands around the Bi(III) was not considered. However the study of other highly charged cations like Po(IV) and Te(IV)^{21,23,56} indicates that a first coordination shell with four OH^- ligands can give rise to two OH^- groups opposite to each other. In this case metal- O_{OH} distances are larger than those found in less hydrolyzed clusters. The same conclusion holds up when the structures of aqueous Bi(III) derived from simulations 3A-3C are analyzed (see Table 1). This arrangement explains the shift toward longer distances found in the Bi-O RDF first peak of simulations 3A-3C in Figure 2.

To test whether a high degree of hydrolysis could lead to the formation of oxo species, simulation 4 was started from the $[\text{BiO}]^+$ aggregate. The results indicate that this oxo species is not stable at all. The Bi-O species evolved to the $[\text{Bi}(\text{OH})]^{2+}$ one during the very initial ~ 9 fs equilibration stage, which means that the protonation of the oxo bond oxygen atom occurred despite the frozen Bi-O distance. In the subsequent run, the system progressed to a chemical distribution of $[\text{Bi}(\text{OH})_2(\text{H}_2\text{O})_3]^+$ and $[\text{Bi}(\text{OH})_2(\text{H}_2\text{O})_4]^+$, something very similar to that of simulation 2B. This shows that all memory of the initial condition has been lost and both simulations reach the same chemical composition.

EXAFS and XANES spectra of Bi(III) aqueous solutions

In Figure 4 we compare some calculated model EXAFS spectra to the experiment. The top panel compares the experimental L_3 -edge k^3 -weighted spectrum of an acidic $\text{Bi}(\text{ClO}_4)_3$ aqueous solution (dotted blue line) with that of a $[\text{Bi}(\text{H}_2\text{O})_9](\text{CF}_3\text{SO}_3)_3$ crystal (dotted black line), both obtained by Näslund et al.¹⁷ The middle panel compares the EXAFS spectrum derived from our AIMD simulation 1 (solid black line) with the experimental one recorded by Naslund et al.¹⁷ for the $\text{Bi}(\text{ClO}_4)_3$ aqueous solution (dotted blue line). The bottom panel shows a spectrum obtained from the classical MD simulation that has used the $[\text{Bi}(\text{H}_2\text{O})_8]^{3+} - \text{H}_2\text{O}$ intermolecular potential specifically fitted to reproduce the structural data reported by Näslund et al.¹⁷ (solid red line). The red curve was obtained from a 250 ps classical MD simulation.

First of all we will analyze the spectra of Bi(III) aqueous solution plotted in the middle panel of Figure 4. The theoretical spectrum from our AIMD simulation (black solid line) has a smaller amplitude and frequency than the experimental one of the $\text{Bi}(\text{ClO}_4)_3$ aqueous solution (dotted blue line). If this was an analysis of single scattering signals, it would indicate that our AIMD simulation has a smaller coordination number and/or a larger DW factor. However in the case of electrolyte solutions this analysis is complicated by the presence of counterions and concentration. Only in very dilute solution can we be sure that counterion effects do not disturb the ion solvation structure. Our simulated spectrum corresponds to the high-dilution limit as our AIMD simulation 1 describes a single Bi(III) only surrounded by water molecules with a dominant backscattering contribution due to the first-shell Bi- $\text{O}_{\text{H}_2\text{O}}$ paths. This is confirmed by the simple shape of the EXAFS function (black line in the middle of Figure 4) that corresponds to an average $R_{\text{Bi}-\text{O}_1} = 2.47 \pm 0.2$ Å. By contrast the experimental EXAFS spectrum of the 0.66M $\text{Bi}(\text{ClO}_4)_3$ aqueous solution recorded by Näslund et al.¹⁷ was modeled by a fitting which included contributions to the EXAFS signal not only from the first-shell Bi- $\text{O}_{\text{H}_2\text{O}}$ paths but also from the Bi- O_{ClO_4} and the second-shell Bi-O paths. In that case, the fitted first-shell $R_{\text{Bi}-\text{O}_1}$ was 2.41Å.

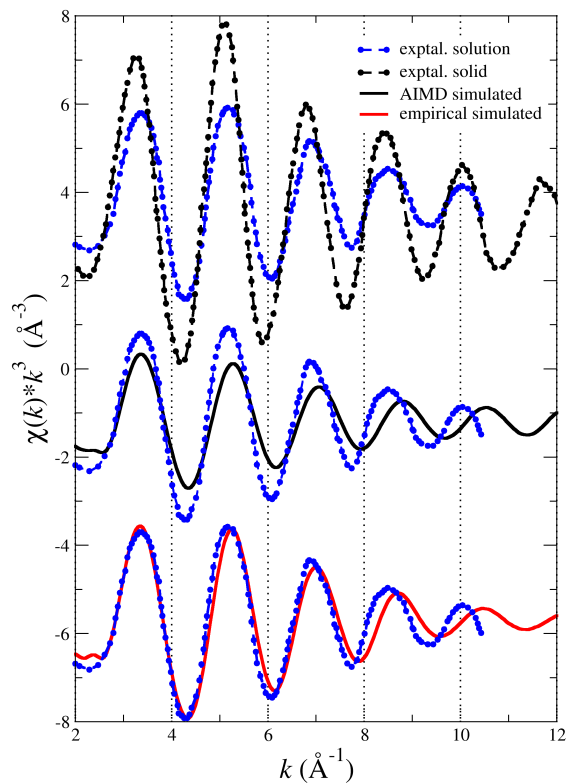


Figure 4: Comparison of experimental k^3 -weighted EXAFS spectra of a Bi(III) perchlorate aqueous solutions (blue dotted line) with solid hydrate $[\text{Bi}(\text{H}_2\text{O})_9](\text{CF}_3\text{SO}_3)_3$ (black dotted line)¹⁷ (top), with simulated spectrum derived from the AIMD simulation of Bi(III) in water (black line) (middle), and with the simulated spectrum obtained from a classical MD simulation using an ad-hoc intermolecular Bi-water potential fitted to reproduce the structural data given by the experimental fitting (red line) (bottom).

Looking at the top panel of Figure 4, the higher amplitude of the $[\text{Bi}(\text{H}_2\text{O})_9](\text{CF}_3\text{SO}_3)_3$, solid sample (black dotted line) with respect to the experimental spectrum of the liquid sample reflects two features discriminating both systems: i) the coordination number for the solid sample is higher than for the liquid one, ii) the DW factor is smaller for the solid sample than for the liquid one. The frequency of their EXAFS signals is quite similar even though $R_{\text{Bi-O}}$ in the crystal is 0.08 Å longer than in the solution.¹⁷ Although $R_{\text{Bi-O}}=2.49$ Å in the solid is quite close to our AIMD simulation value, the signal frequency is rather different for both spectra. The bottom panel of Figure 4 shows a second experimental-theoretical comparison of the EXAFS liquid sample (blue dotted line) with the simulated spectrum (red line) obtained from a classical MD simulation which used the ad-hoc classical interaction potential previously described. In this case, the simple signal provided by the simulated EXAFS (red line) exhibits a frequency lower than that of the experimental signal solution (blue dotted line), although structurally for both samples $R_{\text{Bi-O}_1} = 2.408$ Å. Following Näslund et al.'s analysis, the difference between these EXAFS signals is due to two additional contributions coming from the presence of one perchlorate anion in the first-shell and the second hydration shell. Addition of a second hydration shell in the EXAFS modeling from our AIMD simulation makes little difference to the shape of the predicted spectra.

Tooth et al.¹⁹ provided an independent XANES spectrum of the Bi(III) aqua ion at high T and P (see Figure 5 dotted line). Because the low liquid compressibility and sensitivity of XANES to pressure, it is reasonable to compare the computed XANES from simulation 1, the Bi(III) aqua ion, (red line) with the experimental one. To match the position of the main resonance, the theoretical spectrum has been only shifted -4.5 eV. For the sake of completeness, the MD trajectory derived from the use of the classical Bi-H₂O intermolecular potential has been used to simulate a second XANES spectrum. The good agreement of both simulated spectra with the experimental one supports the reliability of the structural description derived from the AIMD and classical MD simulations.

Further to the the Bi(III) aqua ion EXAFS spectrum, we extended our study to the

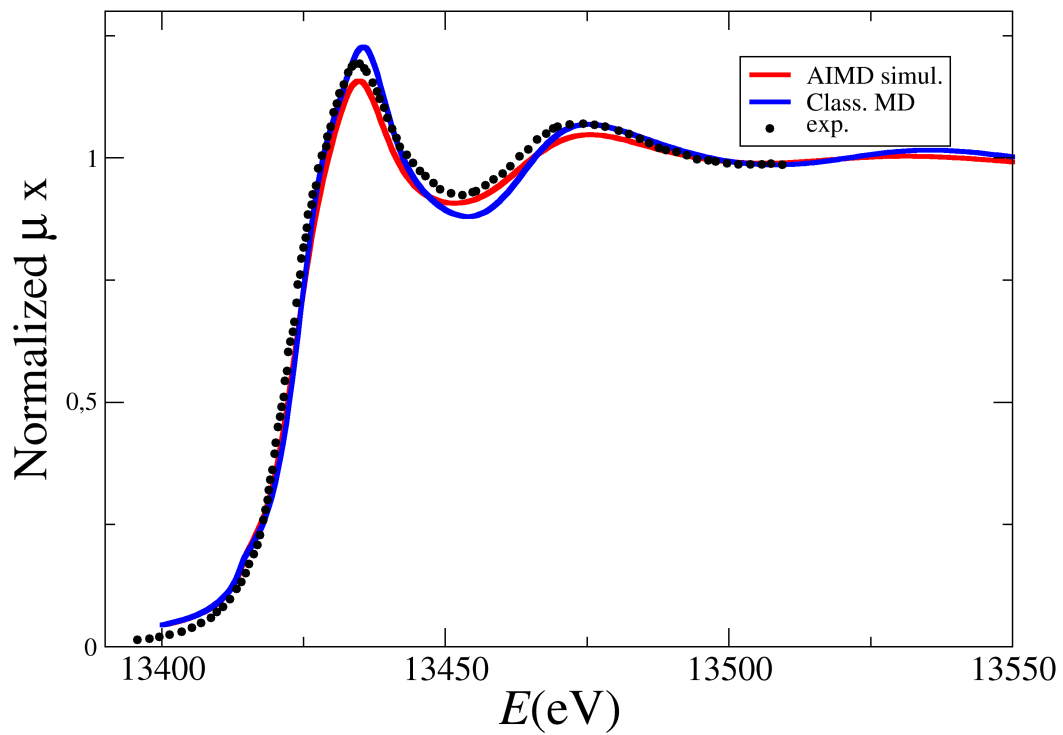


Figure 5: Experimental (dotted line) (taken from ref.[19]) XANES spectrum of Bi(III) aqueous solutions and simulated ones obtained from the AIMD (red line) or the classical MD trajectories (blue line)

spectroscopic features of hydrolyzed species. We computed the simulated EXAFS spectra of the mono-, di- and tri-hydrolyzed Bi(III) aqua ion from simulation 2A, 2B and 2C, respectively (see Table 2) by selecting trajectories where a specific Bi(III) aqua ion degree of hydrolysis is dominant in solution. Figure 6 displays the simulated EXAFS spectra (black solid line) of these three hydrolyzed forms. It is clear that the shapes are different enough to support EXAFS as a tool to discriminate among different hydrolyzed forms, and from the non-hydrolyzed species already examined in Figure 4. In the case of the hydrolyzed form, Tooth et al.¹⁹ have recorded the experimental spectrum under hydrothermal conditions of Bi(OH)₃ (green line on the bottom of Figure 6). The comparison with the simulated one from AIMD simulation 2C supports the reasonable theoretical description of the AIMD simulation for the hydrolyzed species. The mono-hydrolyzed species spectrum is characterized by a significant decrease of the amplitude at medium k -values, whereas the di-hydrolyzed spectrum exhibits a monotonous amplitude increase with k , and the tri-hydrolyzed spectrum exhibits a moderate decrease of the amplitude above medium k -values. Figure 6 includes separately the two main contributions to these EXAFS spectra which are the two Bi-O scattering paths due to the hydroxyl ligands and the first-shell water molecules. The relative weight of these two paths changes with the hydroxyl count, as there is not a one-for one substitution for first-shell water molecules.^{21,56} Therefore the mono-hydrolyzed spectrum is a sum of an out-of-phase combination of both contributions bearing a similar intensity. This leads to destructive interference in the medium k -range. For the di-hydrolyzed spectrum, the Bi-O_{H₂O} contribution decreases with respect to that due to the hydroxyl paths, the main out-of-phase effects appearing at low k . Finally the tri-hydrolyzed spectrum is strongly dominated by the Bi-O_{OH} paths and the spectrum shape approaches a simple oscillation decaying with k .

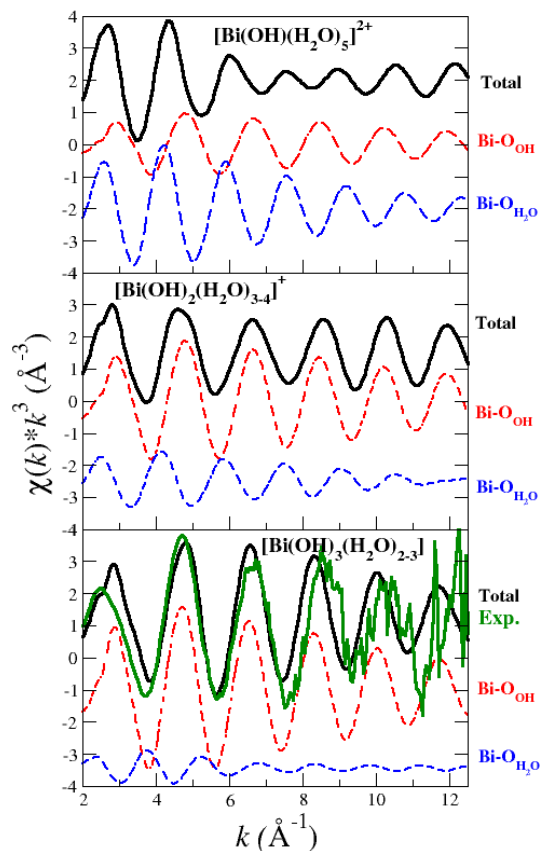


Figure 6: Simulated EXAFS spectra of Bi(III) aqueous solutions under different degrees of hydrolysis and their two main contributions due to the Bi-O_{OH} and Bi-O_{H₂O}. Experimental EXAFS spectrum for Bi(OH)₃ taken from Tooth et al.¹⁹(green line, bottom)

Concluding Remarks.

We examined the aqueous solvation structure of Bi(III) ion using AIMD based on DFT (PBE/GGA) over a wide range of basicity by including different numbers of hydroxide anions. Our results show a strong dependence of the composition of the Bi(III) first solvation shell with basicity. The increase in the alkalinity not only facilitates hydrolysis reactions but also the dehydration processes. This behaviour is less pronounced than that found in our previous quantum mechanical study²¹ likely due to the added feature of an explicit description of the bulk solvent. In this case the coordination number does not decrease with increasing hydrolysis but reaches an asymptotic value around 5-6 in simulation 2B that persists even when the degree of basicity increases in the simulation cell (simulation 3C).

The preference for the hydroxyl ligands to avoid themselves in a *trans* configuration, found in a previous semi-continuum solvent model study,²¹ was now confirmed from fully explicit solvent simulations. However, there are some discrepancies with experimental evidence regarding the highest degree of hydrolysis that can be reached. The species distribution diagram (Figure 1) shows the $[\text{Bi}(\text{OH})_4]^-$ species as the one present at extreme alkaline conditions, whereas our results go further, and predict $[\text{Bi}(\text{OH})_5]^{2-}$ and $[\text{Bi}(\text{OH})_6]^{3-}$ aggregates.

Experimentally, mononuclear Bi(III) species are only formed in dilute aqueous solution. Although the use of just one single ion in our simulation boxes guarantees the lack of polynuclear aggregates, current computational resources still constrain the ion/water ratio to be several orders of magnitude greater than pertains in dilute solution. The buffering effect of the solvent in a real solution is reduced by the small number of water molecules included in our study. Nevertheless the results show that the AIMD methodology is sensitive to the change of acidity. But a quantitative prediction of the hydrolysis/pH relationship will require further developments. It is also necessary to consider that the experimental phase diagram predicts the aqua ion not only at very dilute conditions but also at very acidic conditions ($\text{pH} < 1$). Our results predict the aqua ion to be a stable species in simulations where no protons were added or removed. This implies that our model using the PBE functional

describes a medium at more acidic conditions than prevail in reality. These concerns should not overshadow the value of the AIMD technique to provide information on the relationship between the acidity/basicity in solution and the nature of the close environment of the metal ions.

The simulated EXAFS spectrum for each hydrolyzed forms of Bi(III) aqua ion was computed from the corresponding structural information provided by the AIMD simulation where that species is dominant. This demonstrates a clear sensitivity of the EXAFS signal to the degree of hydrolysis. The shape of the spectrum is dominated by the different weights of the Bi-O_{OH} and Bi-O_{H₂O} single-scattering contributions borne by the different hydrolyzed species. For the Bi(III) aqua ion a direct comparison of the correspondence between theoretical and experimental EXAFS spectra is not possible as the solution conditions are different, but the observed differences can be understood. The experimental-theoretical comparison for the XANES spectrum of the Bi(III) aquaion is satisfactory, as well as that of the EXAFS spectrum corresponding to the tri-hydrolyzed species. This supports the structural reliability of our simulations.

Supporting Information

Bi-O RDF error analysis. O(OH)-O(H₂O) RDFs. Feff input files for EXAFS spectrum computations.

Acknowledgments

We would like to thank Prof. I. Persson, University of Uppsala and Prof. J.Brugger and Dr. B. Etschmann, University of Adelaide, for sending us the experimental EXAFS spectra. Junta de Andalucia is acknowledged for financial support (Proyecto de Excelencia P11-FQM7607).

References

- (1) Jr. Baes, G. F.; Mesmer, R. E. *The Hydrolysis of Cations*; Wiley and Sons: New York, 1976.
- (2) Ritchens, D. *The Chemistry of Aqua Ions*; Wiley: Chichester, 1997.
- (3) Marcus, Y. *Ions in Solution and their Solvation*; Wiley: Hoboken, New Jersey, 2015.
- (4) Tytko, K. Isopolyozokationen-Metallkationen in wäßriger Lösung. *Chemie in Unserer Zeit*. **1979**, *13*, 184.
- (5) Brown, P. L.; Ekberg, C. *Hydrolysis of Metal Ions*; Wiley-VCH: Weinheim, Germany, 2016.
- (6) Martell, A. E.; Smith, R. M.; Motekaitis, R. J. NIST Standard Reference Database 46 Version 8.0. NIST Critically Selected Stability Constants of Metal Complexes Database. Gaithersburg, USA, 2004.
- (7) Greenwood, N. N.; Earnshaw, A. *Chemistry of the Elements*; Butterworth: UK, 1997.
- (8) Yang, N.; H. Sun, Biocoordination chemistry of bismuth: Recent advances. *Coord. Chem. Rev.* **2007**, *251*, 2354–2366.
- (9) Bidleman, T. F. Bismuth-dithizone equilibria and hydrolysis of bismuth ion in aqueous solution. *Anal. Chim. Acta* **1971**, *56*, 221–231.
- (10) Stuart Tobias, R. Studies on hydrolyzed bismuth(III) solutions. Part I. e.m.f. titrations. *J. Am. Chem. Soc.* **1960**, *82*, 1070–1072.
- (11) Kragten, J.; Decnop-Weever, L. G.; Gründler, P. Mixed hydroxide complex-formation and solubility of bismuth in nitrate and perchlorate medium. *Talanta* **1993**, *40*, 485–490.

- (12) Oertel, R. P.; Plane, R. A. Raman and infrared study of nitrate complexes of bismuth(III). *Inorg. Chem.* **1968**, *7*, 1192–1196.
- (13) Suganuma, H.; Ono, K.; Hataye, I. A cation-exchange study of stability-constants of complexes formed between bismuth-III and nitrate or chloride-ions. *J. Radioanal. Nucl. Chem.-Letters* **1990**, *145*, 167–173.
- (14) Johansson, L. The Complex Formation of Bismuth(III) with Chloride in Aqueous Solution. A Solubility Study. *Acta Chem. Scand.* **1969**, *23*, 548–556.
- (15) Newman, L.; Hume, D. N. A Spectrophotometric Study of the Bismuth-Chloride Complexes. *J. Am. Chem. Soc.* **1957**, *79*, 4576–4581.
- (16) Billing, C.; Cukrowski, I. Measurements and Modeling To Determine the Reduction Potential of Uncomplexed Bi(III) in Nitrate Solutions for Application in Bi(III)-Ligand Equilibria Studies by Voltammetry. *J. Phys. Chem. B* **2016**, *120*, 4268–4278.
- (17) Näslund, J.; Persson, I.; Sandström, M. Solvation of the Bismuth(III) Ion by Water, Dimethyl Sulfoxide, N,N-Dimethylpropyleneurea, and N,N-Dimethylthioformamide. An EXAFS, Large-Angle X-ray Scattering, and Crystallographic Structural Study. *Inorg. Chem.* **2000**, *39*, 4012–4021.
- (18) Pye, C. C.; Gunasekara, M.; Rudolph, W. W. An ab initio investigation of bismuth hydration. *Can. J. Chem.* **2007**, *85*, 945–950.
- (19) Tooth, B.; Etschmann, B.; Pokrovski, G.; Testemale, D.; Hazemann, J.-L.; Grundler, P.; Brugger, J. Bismuth Speciation in Hydrothermal Fluids: An X-ray Absorption Spectroscopy and Solubility Study. *Geochim. Cosmochim. Acta* **2013**, *101*, 156–172.
- (20) Tooth, B. The Hydrothermal Chemistry of Bismuth and The Liquid Bismuth Collector Model. Ph.D. thesis, University of Adelaide,

(<https://digital.library.adelaide.edu.au/dspace/bitstream/2440/83112/8/02whole.pdf>), 2013.

- (21) Ayala, R.; Martínez, J. M.; Pappalardo, R. R.; Sánchez Marcos, E. Quantum-Mechanical Study on the Aquaions and Hydrolyzed Species of Po(IV), Te(IV), and Bi(III) in Water. *J. Phys. Chem. B* **2012**, *116*, 14903–14914.
- (22) Tomasi, J.; Mennucci, B.; Cammi, R. Quantum Mechanical Continuum Solvation Models. *Chem. Rev.* **2005**, *105*, 2999–3093.
- (23) Ayala, R.; Spezia, R.; Vuilleumier, R.; Martínez, J. M.; Pappalardo, R. R.; Sánchez Marcos, E. An Ab Initio Molecular Dynamics Study on the Hydrolysis of the Po(IV) Aquaion in Water. *J. Phys. Chem. B* **2010**, *114*, 12866–12874.
- (24) Guillan, M. J.; Alfe, D.; Michaelides, A. Perspective: How good is DFT for water? *J. Chem. Phys.* **2016**, *144*, 130901.
- (25) Kuo, I. W.; Mundy, C. J.; McGrath, M. J.; Siepmann, J. I.; VandeVondele, J.; Sprik, M.; Hutter, J.; Chen, B.; Klein, M. L.; Mohamed, F. et al. Liquid Water from First Principles: Investigation of Different Sampling Approaches. *J. Phys. Chem. B* **2004**, *108*, 12990–12998.
- (26) McGrath, M.; Siepmann, J. I.; Kuo, I. W.; Mundy, C. J.; VandeVondele, J.; Hutter, J.; Mohamed, F.; Krack, M. IsobaricIsothermal Monte Carlo Simulations from First Principles: Application to Liquid Water at Ambient Conditions. *Chem. Phys. Chem.* **2005**, *6*, 1894–1901.
- (27) Corsetti, F.; Artacho, E.; Soler, J.; Alexandre, S.; Frenandez-Serra, M. V. Room temperature compressibility and diffusivity of liquid water from first principles. *J. Chem. Phys.* **2013**, *139*, 194502.

- (28) Wang, J.; Roman-Perez, G.; Soler, J. M.; Artacho, E.; Fernandez-Serra, M. V. Density, structure, and dynamics of water: The effect of van der Waals interactions. *J. Chem. Phys.* **2011**, *134*, 059901.
- (29) Lin, I.; Seitsonen, A. P.; Tavernelli, I.; Rothlisberger, U. Structure and Dynamics of Liquid Water from ab Initio Molecular Dynamics Comparison of BLYP, PBE, and revPBE Density Functionals with and without van der Waals Corrections. *J. Chem. Theory Comput.* **2012**, *8*, 39023910.
- (30) Miceli, G.; Gironcoli, S.; Pasquarello, A. Isobaric first-principles molecular dynamics of liquid water with nonlocal van der Waals interactions. *J. Chem. Phys.* **2015**, *142*, 034501.
- (31) Soper, A.; Bruni, F.; Ricci, M. Site-site pair correlation functions of water from 25 to 400 degrees C: Revised analysis of new and old diffraction data. *J. Chem. Phys.* **1997**, *106*, 247–254.
- (32) Tuckerman, M. E.; Chandra, A.; Marx, D. Structure and Dynamics of OH⁻(aq). *Acc. Chem. Res.* **2006**, *39*, 151–158.
- (33) Marx, D.; Chandra, A.; Tuckerman, M. E. Aqueous Basic Solutions: Hydroxide Solvation, Structural Diffusion and Comparison to the Hydrated Proton. *Chem. Rev.* **2010**, *110*, 2174–2216.
- (34) Agmon, N.; Bakker, H. J.; Campen, R. K.; Henchman, R. H.; Pohl, P.; Roke, S.; Thämer, M.; Hassanali, A. Proton and Hydroxide Ions in Aqueous Systems. *Chem. Rev.* **2016**, *116*, 7642–7672.
- (35) Muñoz-Páez, A.; Sánchez Marcos, E. Molecular Structure of Solvates and Coordination Complexes in Solution as Determined with EXAFS and XANES. *Comprehensive Inorganic Chemistry II: From Elements to Applications* **2013**, *9*, 133–159.

- (36) Filipponi, A.; D'Angelo, P.; Pavel, N. V.; Di Cicco, A. Triplet correlations in the hydration shell of aquaions. *Chem. Phys. Lett.* **1994**, *225*, 150–155.
- (37) Palmer, B. J.; Pfund, D. M.; Fulton, J. L. Direct modeling of EXAFS spectra from molecular dynamics simulations. *J. Phys. Chem.* **1996**, *100*, 13393–13398.
- (38) Campbell, L.; Rehr, J.; Schenter, G. K.; McCarthy, M. I.; Dixon, D. XAFS Debye-Waller factors in aqueous Cr^{+3} from molecular dynamics. *J. Synchrotron Radiat.* **1999**, *6*, 310–312.
- (39) Jalilehvand, F.; Spångberg, D.; Lindqvist-Reis, P.; Hermansson, K.; Persson, I.; Sandström, M. Hydration of the Calcium Ion. An EXAFS, Large-Angle X-ray Scattering, and Molecular Dynamics Simulation Study. *J. Am. Chem. Soc.* **2001**, *123*, 431–441.
- (40) Merklings, P. J.; Muñoz-Páez, A.; Sánchez Marcos, E. Exploring the Capabilities of X-ray Absorption Spectroscopy for Determining the Structure of Electrolyte Solutions: Computed Spectra for Cr^{3+} or Rh^{3+} in Water Based on Molecular Dynamics. *J. Am. Chem. Soc.* **2002**, *124*, 10911–10920.
- (41) Car, R.; Parrinello, M. Unified Approach for Molecular-Dynamics and Density-Functional Theory. *Phys. Rev. Lett.* **1985**, *55*, 2471–2474.
- (42) CPMD, Copyright IBM Corp 1990-2015, Copyright MPI für Festkörperforschung Stuttgart 1997-2001.
- (43) Nosé, S. A unified formulation of the constant temperature molecular dynamics methods. *J. Chem. Phys.* **1984**, *81*, 511–519.
- (44) Nosé, S. A Molecular-Dynamics Method for Simulations in the Canonical Ensemble. *Mol. Phys.* **1984**, *52*, 255–268.
- (45) Hoover, W. G. Canonical Dynamics-Equilibrium Phase-Space Distributions. *Phys. Rev. A* **1985**, *31*, 1695–1697.

- (46) Vanderbilt, D. Soft Self-consistent Pseudopotentials in a Generalized Eigenvalue Formalism. *Phys. Rev. B* **1990**, *41*, 7892–7895.
- (47) Perdew, J.; Burke, K.; Ernzerhof, M. Generalized Gradient Approximation Made Simple. *Phys. Rev. Lett.* **1996**, *77*, 3865–3868.
- (48) Lejaeghere, K.; Bihlmayer, G.; Bjrkman, T.; Blaha, P.; Blgel, S.; Blum, V.; Caliste, D.; Castelli, I. E.; Clark, S. J.; Corso, A. D. et al. Reproducibility in density functional theory calculations of solids. *Science* **2016**, *351*, aad3000.
- (49) Beret, E. C.; Pappalardo, R. R.; Doltsinis, N. L.; Marx, D.; Sánchez Marcos, E. Aqueous Pd^{II} and Pt^{II}: Anionic Hydration Revealed by CarParrinello Simulations. *ChemPhysChem* **2008**, *9*, 237–240.
- (50) Berendsen, H. J. C.; Griger, J. R.; Straatsma, T. P. The missing term in effective pair potentials. *J. Phys. Chem.* **1987**, *91*, 6269–6271.
- (51) D’Angelo, P.; Barone, V.; Chillemi, G.; Sanna, N.; Meyer-Klauche, W.; Pavel, N. V. Hydrogen and Higher Shell Contributions in Zn²⁺, Ni²⁺, and Co²⁺ Aqueous Solutions: An X-ray Absorption Fine Structure and Molecular Dynamics Study. *J. Am. Chem. Soc.* **2002**, *124*, 1958–1967.
- (52) Carrera, F.; Torrico, F.; Richens, D. T.; Muñoz-Paez, A.; Martínez, J. M.; Pappalardo, R. R.; Sánchez Marcos, E. Combined Experimental and Theoretical Approach to the Study of Structure and Dynamics of the Most Inert Aqua Ion [Ir(H₂O)₆]³⁺ in Aqueous Solution. *J. Phys. Chem. B* **2007**, *111*, 8223–8233.
- (53) Rehr, J. J.; Kas, J. J.; Vila, F. D.; Prange, M. P.; Jorissen, K. Parameter-free calculations of x-ray spectra with FEFF9. *Phys. Chem. Chem. Phys.* **2010**, *12*, 5503–5513.
- (54) Provost, K.; Beret, E. C.; Bouvet-Muller, D.; Michalowicz, A.; Sánchez Marcos, E.

- EXAFS Debye-Waller Factors Issued from Car-Parrinello Molecular Dynamics: Application to the Fit of Oxaliplatin and Derivatives. *J. Chem. Phys.* **2013**, *138*, 084303.
- (55) Holovko, M.; Drucho, M.; Bryk, T. A molecular dynamics modelling of cation hydrolysis effects. *J. Electroanal. Chem.* **2005**, *582*, 50–56.
- (56) Ayala, R.; Martínez, J. M.; Pappalardo, R. R.; Muñoz-Paez, A.; Sánchez Marcos, E. General Quantum-Mechanical Study on the Hydrolysis Equilibria for a Tetravalent Aquaion: The Extreme Case of the Po(IV) in Water. *J. Phys. Chem. B* **2009**, *113*, 487–496.
- (57) Tsushima, S. General Quantum-Mechanical Study on the Hydrolysis Equilibria for a Tetravalent Aquaion: The Extreme Case of the Po(IV) in Water. *J. Phys. Chem. B* **2008**, *113*, 7080–7085.
- (58) Flyvberg, H.; Petersen, H. G. Error Estimates on Averages of Correlated Data. *J. Chem. Phys.* **1989**, *91*, 461–466.
- (59) Crespo, Y.; Hassanali, A. Characterizing the Local Solvation Environment of OH⁻ in Water Clusters with AIMD. *J. Chem. Phys.* **2016**, *144*, 074304.
- (60) Khan, A.; Weiss, A. K. H.; Uddin, R.; Randolph, B. R.; Rode, B. M.; Hofer, T. S. Ab Initio Quantum Mechanical Charge Field Molecular Dynamics Simulation (QMCF-MD) of Bi³⁺ in Water. *J. Phys. Chem. A* **2012**, *116*, 8008–8014.

TOC Graphic

